ADVANCED MATERIALS
www.advmat.de

Few-Layer Black Phosphorus Carbide Field-Effect Transistor via Carbon Doping

*Wee Chong Tan, Yongqing Cai, Rui Jie Ng, Li Huang, Xuewei Feng, Gang Zhang, Yong-Wei Zhang, Christian A. Nijhuis, Xinke Liu, and Kah-Wee Ang**

Black phosphorus carbide (b-PC) is a new family of layered semiconducting material that has recently been predicted to have the lightest electrons and holes among all known 2D semiconductors, yielding a p-type mobility (≈10^5 cm^2 V^{-1} s^{-1}) at room temperature that is approximately five times larger than the maximum value in black phosphorus. Here, a high-performance composite few-layer b-PC field-effect transistor fabricated via a novel carbon doping technique which achieved a high hole mobility of 1995 cm^2 V^{-1} s^{-1} at room temperature is reported. The absorption spectrum of this material covers an electromagnetic spectrum in the infrared regime not served by black phosphorus and is useful for range finding applications as the earth atmosphere has good transparency in this spectral range. Additionally, a low contact resistance of 289 Ω μm is achieved using a nickel phosphide alloy contact with an edge contacted interface via sputtering and thermal treatment.

Recent years have witnessed many breakthroughs in research on 2D layered materials (2DMs). Materials such as graphene,[1,2] transition metal dichalcogenides (TMDC),[3] hexagonal BN (h-BN),[4] black arsenic phosphorus (b-AsP),[5] and black phosphorus (b-P),[6] are all examples of 2DMs that may have an impact in radio frequency, infrared, ultralow power, and high-speed flexible electronics and photonics[7] technologies in the coming years. Unlike graphene, h-BN, and TMDC, b-P is a 2D layered semiconductor with high carrier mobility and an intrinsic tunable bandgap ranging from 2.0 eV for monolayer to 0.3 eV for bulk b-P. It is also an emerging infrared and mid-infrared optical material.[8] Experimentally, various top-gated and bottom-gated b-P based field-effect transistors (FET) utilizing different gate dielectrics,[9] metal contacts,[10,11] and encapsulation layers[12,13] have been reported but the room-temperature p-type field-effect (FE) mobility still hovers below 1000 cm^2 V^{-1} s^{-1}.[11,14–19] Although this FE mobility can be increased to 5200 cm^2 V^{-1} s^{-1}, the process requires the mechanical stacking of Van der Waals heterostructure materials in vacuum rather than at atmospheric pressure.[12] On the other hand, b-AsP is a new family of layered semiconducting materials that despite its relatively lower hole mobility at 110 cm^2 V^{-1} s^{-1}, can fill up a technologically important gap in the long-wavelength infrared (LWIR) regime of the electromagnetic spectra, which cannot be readily served by other 2D layered materials. This particular electromagnetic spectral range is important for a range of applications such as range finding using LIDAR (light radar) systems because the earth atmosphere (mostly H_2O, O_3, and CO_2) has good transparency in this spectral range.[5] Similarly, black phosphorus carbide (b-PC) is another new family of layered semiconducting materials that has recently been predicted due to the structural similarities between graphene and phosphorene.[20,21] As per the studies, there are three geometrically different phases of b-PC monolayer within each category of b-PC with the same number of nearest like-neighbors. More importantly, two of these phases with puckered surfaces have the lightest electrons and holes among all the known 2D semiconductors, yielding a p-type mobility at room temperature that could potentially reach 1.15×10^5 cm^2 V^{-1} s^{-1}. This mobility is approximately five times larger than the maximum value in b-P. Not only is the mobility higher, its band structure is also different from b-P and b-AsP. Depending on its composition, b-PC can have a band structure that is metallic, semimetallic with an anisotropic Dirac cone, or direct gap semiconductors with a bandgap ranging from those in b-AsP to those found in b-P.[20,21] Although several experimental efforts have already been made to produce and establish the presence of direct P—C bonds in phosphorus carbide amorphous films, no group has yet reported a 2D b-PC few-layer crystalline material.[22,23]

Here, we report on a high-performance composite few-layer b-PC p-FET fabricated via a novel carbon doping technique which achieved a high mobility of 1995 cm^2 V^{-1} s^{-1} at room temperature. First principles calculations show a stable b-PC with an effective mass of carriers that is lighter than b-P along

Dr. W. C. Tan, R. J. Ng, L. Huang, X. Feng, Prof. K.-W. Ang
Department of Electrical and Computer Engineering
National University of Singapore
4 Engineering Drive 3, 117583 Singapore
E-mail: eleakw@nus.edu.sg
Dr. Y. Cai, Dr. G. Zhang, Prof. Y.-W. Zhang
Institute of Higher Performance Computing
1 Fusionopolis Way, 138632 Singapore
Prof. C. A. Nijhuis
Department of Chemistry
NUS
3 Science Drive 3, 117543 Singapore
Dr. X. Liu
College of Materials Science and Engineering
Guangdong Research Center for Interfacial
Engineering of Functional Materials
Shenzhen University
3688 Nanhai Ave, Shenzhen 518060, P. R. China

DOI: 10.1002/adma.201700503

the armchair direction and a bandgap in the LWIR regime. Raman spectroscopy, energy dispersive X-ray (EDX) spectroscopy, X-ray photoelectron spectroscopy (XPS), and the time of flight secondary ion mass spectrometry (TOF-SIMS) have all been used to characterize and confirm the presence of a b-PC channel in the transistor. Low-temperature transport measurement of the b-PC p-FET revealed a conductivity that is semimetallic at $T < 100$ K, which is different from b-P p-FET, and a transportation limited by optical phonon scattering at $T > 100$ K. Besides the channel, we have also successfully lowered the contact resistance of the b-PC p-FET to 289 Ω μm via an edge contacted metal/b-P interface at the source/drain created by sputtering and a NiP alloy contact formed by thermal annealing. Our results suggest that a family of new layered semiconductors with anisotropic high mobility and tunable bandgaps in the LWIR regime can be synthesized from b-P via carbon doping. We envision that this family of new layered semiconductors will eventually reach a mobility higher than b-P and find unique applications for electronic and optoelectronic devices operating in the infrared regime.

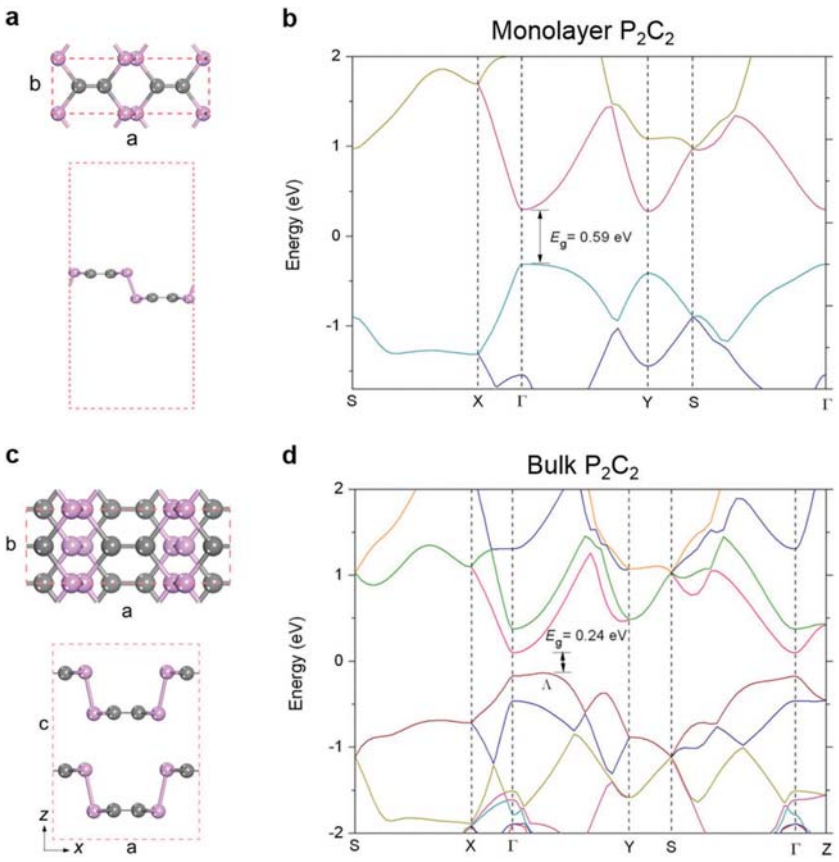

Figure 1. DFT Calculations of monolayer and bulk P_2C_2. a) The top and side views of the monolayer P_2C_2 sheet. b) Band structure of the P_2C_2 sheet. c) The side and top views of the bulk P_2C_2. d) Band structure of the bulk P_2C_2. Note that the peak of the valence band is at the Λ point between Γ and Y points.

To study the formation and physical properties of this new layered semiconductor, we have performed first-principles calculations on a few-layer b-PC. The calculations are conducted within the framework of the density functional theory (DFT) using the Vienna Ab initio simulation package (VASP) (see the Supporting Information for details).[24] Since the cohesive energy of b-PC monolayers (1L) with various stoichiometric compositions (P_xC_{1-x}) has been calculated and found to be lower than graphene but higher than phosphorene, it implies that layers of b-PC with different compositions are possible to be synthesized in experiments by controlling the atomic ratio of P to C.[20] We have chosen P_2C_2 among many allotropes of b-PC as a representative of the P-C layered sheet to study the effect of the layered thickness on a b-PC with equal composition of carbon and phosphorus atoms. **Figure 1**a,b shows the atomic and band structures of a monolayer (1L) P_2C_2 (orthorhombic lattice with $a = 8.328$ Å and $b = 2.927$ Å), and is the stable structure based on the previous calculation.[21] To simulate a few-layer b-PC, various stacking possibilities for bulk P_2C_2 (orthorhombic lattice with $a = 8.042$ Å, $b = 2.923$ Å, and $c = 10.763$ Å) and different relative alignments of P_2C_2 layers have been considered in the calculation. We have found the most stable configuration is AB stacking with a half-lattice shift of $b/2$ along b direction as shown in Figure 1c. Figure 1d shows the band structures of this configuration for the bulk P_2C_2. When comparing the band structures of the bulk P_2C_2 in Figure 1d to the monolayer P_2C_2 in Figure 1b, we can see two differences. First, the bandgap decreases from 0.59 eV for 1L P_2C_2 to 0.24 eV for bulk P_2C_2. Second, the peak of the valence band at Γ in 1L P_2C_2 has shifted from Γ to Λ point when it becomes bulk P_2C_2. Thus, we know 1L P_2C_2 is a semiconductor with a direct bandgap while bulk P_2C_2 and few-layer P_2C_2 (Figures S4 to S7 in the Supporting Information) are semiconductors with an indirect bandgap. Despite the differences in bandgap, both band structures show a highly anisotropic behavior at Γ which is due to anisotropic puckered structure of the sheets. Their effective mass of carriers along the X and Y directions is vastly different and is shown in Tables S2–S4 (Supporting Information). The tables show that P_2C_2 (1L–5L) has a smaller effective mass of hole and electron carriers than b-P (1L–5L) in the armchair (x) direction. Finally, the choice of a b-PC with equal composition is deliberate so that another b-PC monolayer with a different stoichiometric composition can be added to simulate a bilayer heterolayer structures of the form, P_2C_2-$C_{1-x}P_x$. This will extend our theoretical study into a heterolayer b-PC structures, which is experimentally a possibility for a few-layer b-PC (not true for a monolayer b-PC) synthesized from b-P via carbon doping (see the Supporting Information for first-principles calculations of a bilayer heterolayer structures).

Next, we will describe the synthesis of the b-PC with a schematic diagram shown in **Figure 2**a. In general, after the mechanical exfoliation of b-P onto a heavily doped Si/SiO_2 substrate, the sample is immediately transferred into the

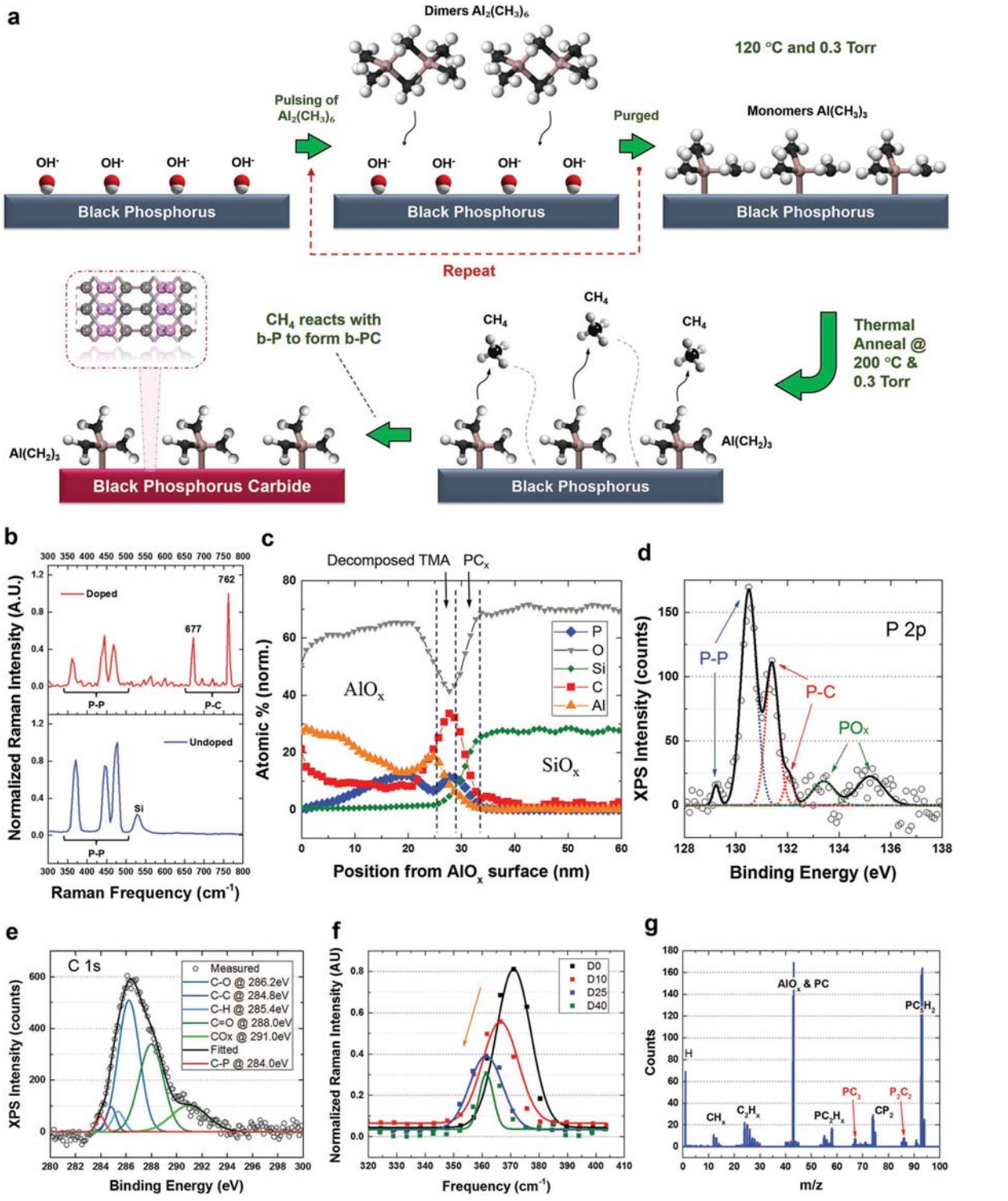

Figure 2. Synthesis of b-PC and material characterization of b-PC. a) Schematic diagram describing the synthesis of phosphorus carbide via ALD of TMA on b-P. b) The Raman spectra of a doped (40 cycles) and undoped few-layer b-PC and b-P, respectively. c) The cross-section energy dispersive X-ray (EDX) spectroscopy of the b-PC channel. d) The XPS spectra of the P 2p core level in b-PC (40 cycles). Besides the crystalline peaks of P-C and P-P, there are also some amorphous peaks PO_x at ≈133.4 and 135.2 eV which are expected when b-P is exposed to the ambient environment.[30] e) The XPS spectra of the C 1s core level binding energy of the b-PC (40 cycles). f) The variation of the out of plane A_g^1 phonon mode with doping cycle. D0 refers to a doping cycle of 0, D10 refers to a doping cycle of 10, D25 refers to a doping cycle of 25, and D40 refers to a doping cycle of 40. g) The TOF-SIMS spectra that show the chemical species of C and PC present in the b-PC (40 cycles). The data presented are raw intensities that can be used to identify a given species in a sample; however, they cannot be used to compare the levels of different species either on the same sample or between samples. This is because different species have different secondary ion yields so TOF-SIMS has different sensitivities for different species.

atomic layer deposition (ALD) chamber where trimethylaluminum (TMA), i.e., $Al_2(CH_3)_6$, precursor is repeatedly pulsed and purged at a substrate temperature of 120 °C and a chamber pressure of 0.3 Torr. At this temperature, the TMA would first adsorb as dimers and then dissociate into monomers upon heating to 120 °C. After metal patterning and deposition, the sample is subjected to another thermal treatment at 200 °C. Further heating of the TMA monomers to 200 °C causes one of the methyl groups in the TMA to react with a hydrogen on another methyl group, liberating methane CH_4. This leaves the CH_2 group bound to the aluminum as a thermally decomposed TMA, $Al_2(CH_2)_6$, and the free radicals CH_4 to react with b-P, breaking the P—P bonds and reorganizing the b-P channel into a b-PC channel (see the Supporting Information for details). The process is consistent with how a TMA will decompose when heat treated at different temperature.[25] Figure 2b shows the Raman spectra of a few-layer b-PC with and without the doping of carbons. Unlike the sample with no doping, the doped sample possesses two prominent phonon modes of b-PC at 677 and 762 cm^{-1}, in addition to the three phonon modes of b-P at 365, 444, and 469 cm^{-1}. The P—C bond stretching modes (670–780 cm^{-1}), are based on theoretical calculations reported in the literature.[23,26] The doping effect of the TMA on the b-P is also evident in Figure 2f, where the Raman intensity and frequency of the out of plane phonon mode, A_g^1, in b-PC have respectively shown to decrease and red-shifted with the number of doping cycles. It indicates that the out of plane P—P bonding structure of the b-P has been chemically modified by the carbon dopants (see layer dependent Raman scattering in the Supporting Information for details). The EDX spectrograph in Figure 2c shows the cross-section channel profile of the b-PC p-FET. From the spectrograph, we can confirm the presence of the Al_2O_3 passivation layer (≈23 nm), the decomposed TMA layer (≈4 nm), and a high concentration of carbon in the few-layer b-PC (≈6 nm). The atomic concentration of carbon (≈35%) is three times higher than phosphorus (≈10%) and is found to peak at the TMA/b-PC interface and slowly decrease along the b-PC thickness toward the b-PC/SiO_2 interface. As per our DFT calculations, this high concentration of carbon would result in a composite b-PC channel consisting of a heterolayer b-PC with a stoichiometric composition that depends on the ratio of P to C. The same EDX spectrograph also shows the diffusion path of the displaced phosphorus atoms of b-P in the thermally decomposed TMA layer. The peak of these diffused atoms starts at the TMA/b-PC interface and decreases along the thickness of the TMA toward TMA/Al_2O_3 interface. The phosphorus atoms in the TMA layer would form phosphine, PH_x, with the hydrocarbons in the TMA and outgas further into the Al_2O_3 layer all the way to the surface (see the Supporting Information for additional comments on the Al in the EDX spectrograph and the evidence of phosphine). Figure 2d shows the XPS spectra of the P 2p core level of the b-PC. The binding energy at 131.4 and 132.1 eV can be assigned to the P—C bonds in b-PC based on references related to phosphorus-doped carbon materials.[2,27,28] The b-PC also exhibits the spin-orbit split doublet of an exfoliated b-P at ≈129.2 and 130.5 eV, consistent with previous XPS measurements on b-P bulk crystals.[29] Similarly, the binding energy at 284.0 eV in the XPS spectra of the C 1s core level in Figure 2e can also be assigned to the covalent P—C bonds based on reports on carbon-doped phosphorus material.[26,28] Other than the evidence of P—C bonds from Raman and XPS, the TOF-SIMS spectra in Figure 2g also confirm the presence of some chemical species of phosphorus carbide in the sample. The findings are consistent with our DFT calculations and with other theoretical calculations in the literatures.[20,21] Additional information on the Fourier transform infrared spectroscopy (FTIR) of b-P and b-PC, device stability performance of b-PC FET, and the dependency of bandgap on the carbon concentration in b-PC can be found in the Supporting Information.

To study the electrical performance of the b-PC p-FET, we have fabricated a two terminals FET with a bottom gate and measured it on a probe station at room temperature under ambient condition. **Figure 3**a,b shows the atomic force microscopy (AFM) image of one of the device and the average thickness measured by the AFM (≈7 nm). Figure 3c,d are respectively the transfer characteristic, $I_d - V_g$ curves, and the output characteristic, $I_d - V_d$ curves, of a b-PC p-FET measured at room temperature. While the linear $I_d - V_d$ characteristics in the figure imply that a high-quality Ohmic-like contact have been formed between the metal electrodes and b-PC channel, the transfer characteristic of the b-PC p-FET allows us to extract its intrinsic or peak FE mobility and contact resistance (see the Supporting Information for details). By physically sputtering the channel to create an edge-contact interface and thermally treating the Ni contact into NiP alloy contact on the b-PC p-FET, we have successfully reduced the contact resistance of this Ohmic-like contacts to 289 Ω μm.

Figure 4a shows the nonmonotonic variation of the calculated peak FE mobility with the channel thickness of transistor. We believe that the nonmonotonic variation with the thickness is mainly due to two competing phenomena. First, the charge impurity at the b-PC/SiO_2 interface, which causes mobility to increase with thickness as the influence of the charge impurities at the b-PC/SiO_2 interface diminishes with thickness. This explains the initial sharp increase in the field-effect mobility as the thickness increases from ≈6 to 8 nm. Second, the charge screening from induced carriers and the finite interlayer resistance of the b-PC, which causes the current to decrease with thickness for a device configured as a bottom-gated transistor. The screening effect is easy to understand as any induced carriers traveling in the channel would also inevitably act as a screen and cancel out any electric field emanating from the bottom from inducing more free carriers in the upper layers of the channel. The effect of the finite interlayer resistance of the b-PC FET is subtler as it forces majority of the current, which is injected from the top surface of the channel, to flow in the upper layers of the channel. It indirectly amplifies the screening effect by subjecting more carriers to the upper layers of the b-PC which is experiencing less electric field due to screening from the induced carriers. Therefore, as the samples become thicker from ≈8 nm, more of its current is being screened and thus its overall FE mobility would decrease. By using a top-gated device structure with a layer of high-k dielectric material, one could effectively screen the charge impurities at the interface and remove the influence of the interlayer resistance and charge screening of induced carrier on the carrier mobility. Figure 4b displays the changes of the p-type FE mobility with the number of doping cycles. Such a variation with doping cycles is expected

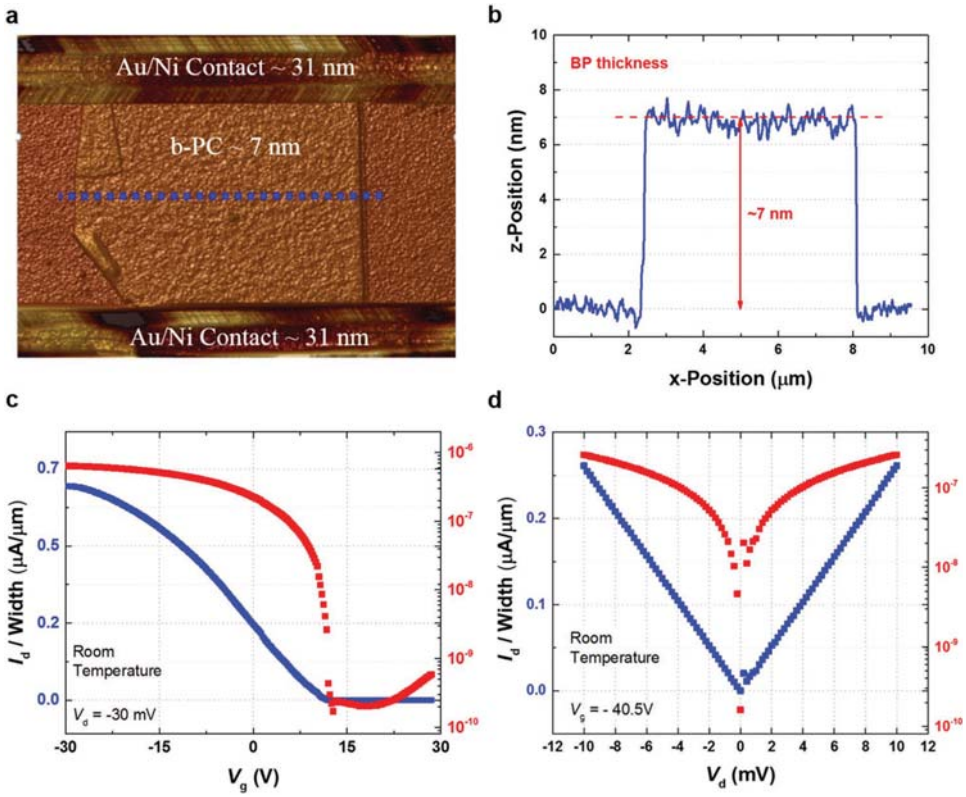

Figure 3. Characterization of b-PC p-FET. a) The atomic force microscopy (AFM) image of one of the b-PC p-FET. b) The AFM measured thickness of the b-PC p-FET shown in panel (a). Average thickness of the b-PC flake is ≈7 nm. c) The room temperature transfers characteristic, I_d–V_g curves, of a 7 nm thick, 5 μm wide and 10 μm long b-PC p-FET plotted in linear (blue) and log scale (red). The doping cycle of this device is 10 and it has a peak field-effect (FE) mobility of 1995 $cm^2\ V^{-1}\ s^{-1}$, an ON/OFF ratio greater than 10^3 and a subthreshold Swing of 1.09 V dec^{-1}. At V_d = -30 mV, the linear drive current I_d = 0.64 μA μm^{-1}. d) The output characteristic, I_d–V_d curves, of the same b-PC p-FET in panel (c) at room temperature plotted in linear (blue) and log scale (red).

as different doping cycle would result in a b-PC with a different stoichiometric composition due to a change in the atomic concentration ratio of P to C. Since each allotrope of b-PC would have a different effective mass, its carrier mobility would thus change with doping cycles. The figure shows that the optimum doping cycle for a 7 nm thick and 5 μm long b-P channel is 25 cycles. Apart from room temperature measurement, we have also conducted a low temperature transport study on the b-PC p-FET (see the Supporting Information for the $I_d - V_g$ curves). Figure 4c portrays a conductivity which is semimetallic at all gating voltages. This is in contrast from a b-P p-FET, where the conductivity for all gating voltages would increase with initial increases in temperature above 2 K before turning around at ≈100–180 K (depending on the gating voltages) and start to decrease.[18] Such a semimetallic behavior is predicted by DFT calculation to exist in one of the allotrope of b-PC.[20,21] As can be seen from Figure 4d, the hole carrier density would increase with the gate voltage and before reaching a high carrier density of $\approx 10^{18}$ cm^{-3} (or a carrier concentration of $\approx 10^{14}$ cm^{-2}) at V_g = –40 V. A carrier concentration above 10^{13} cm^{-2} would imply that two-phonon scattering is negligible and scattering should mostly come from single-phonon scattering with optical phonons.[31] The dependency of FE p-type mobility on the operating temperature (T) is described in Figure 4e. At $T > 100$ K, the FE mobility μ would decrease with increasing temperature and follow an electron–phonon scattering limited transport mechanism. This mechanism has a power law dependence in the form of $\mu \approx T^{-\gamma}$, where the exponent γ depends on the dominant phonon scattering mechanism. A γ value of ≈0.7 was extracted from the linear fit to this part of the curve and the small γ values imply that optical phonon is the dominating scattering event over the scattering of acoustic phonon and residual impurities in this temperature regime. This value is around the value of a homogeneous b-P p-FET[18] (≈0.5) but is smaller than a heterostructure b-P p-FET[12] (≈2.0) encapsulated with h-BN in vacuum. At $T < 100$ K, disorder scattering dominates over the phonon scattering and limits the p-type FE mobility to around ≈1250 $cm^2\ V^{-1}\ s^{-1}$. The disorder potential is most likely generated by residual charged impurities either at the top surface of the b-PC, e.g., Al adatoms, or at the substrate interface, e.g., dangling P or C bonds, and can be improved with interface engineering.[12]

In summary, high-performance few-layer PC p-FETs were demonstrated via a novel carbon doping technique which achieved a high mobility of 1995 $cm^2\ V^{-1}\ s^{-1}$ at room temperature. First-principles calculations predicted a stable b-PC with an effective mass for hole and electron carriers that are lighter than b-P in the armchair direction. EDX profile reveals a b-PC channel full of carbon, Raman and XPS established the P—C bonds that these carbons formed with phosphorus, and

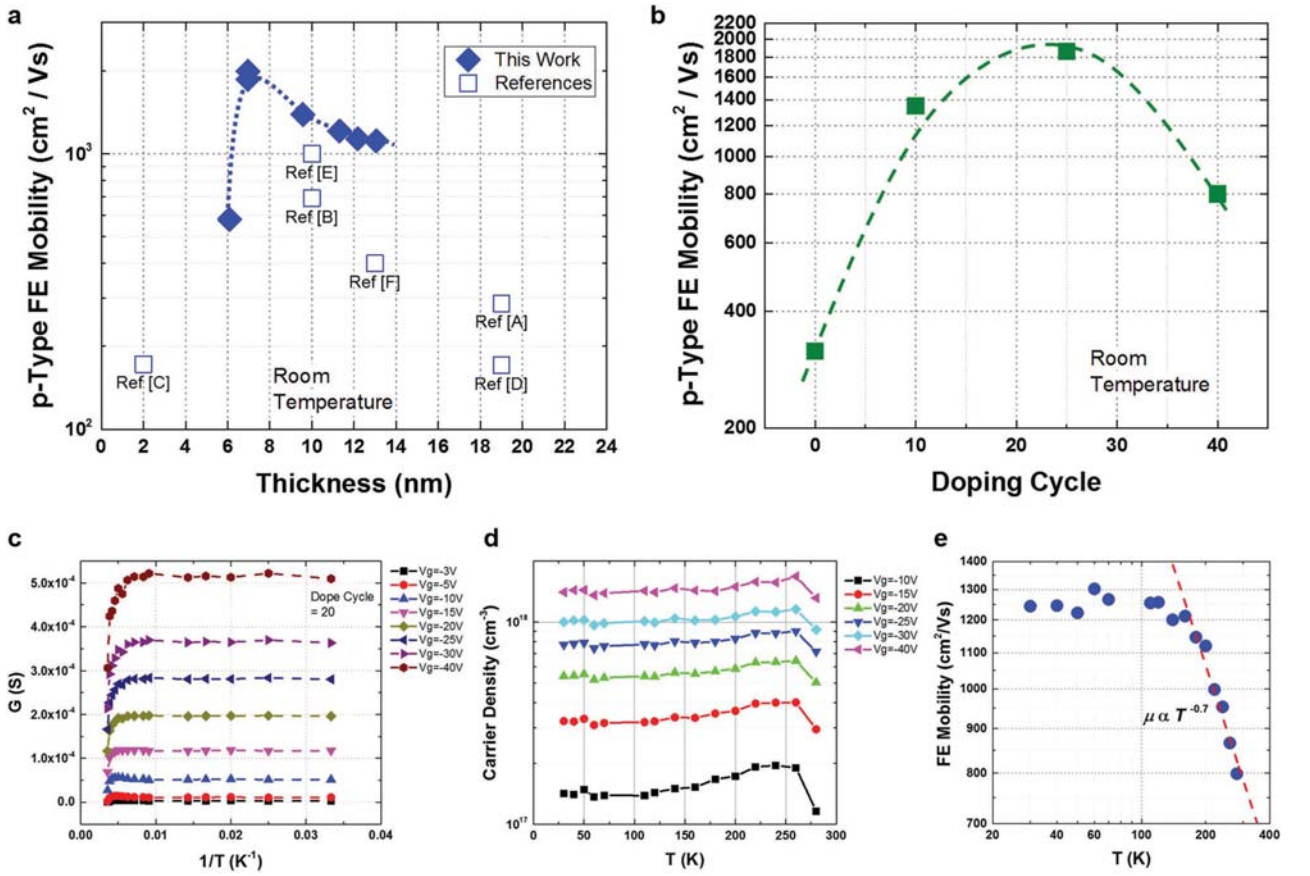

Figure 4. Electrical characterization of b-PC p-FET. a) The p-type FE mobility as a function of the channel thickness of the b-PC p-FET and the comparison to reference values reported in the literature as follows: Ref A,[13] Ref B,[15] Ref C,[16] Ref D,[17] Ref E,[18] and Ref F.[19] The dotted line is drawn as an eye guide to the trend of the mobility with channel thickness. b) The p-type FE mobility of a 7 nm thick and 5 µm long b-PC p-FET at different doping cycles of TMA. The dashed line is drawn as an eye guide to the trend. c) The calculated conductance (G) as a function of temperature (T) measured at various back gate voltage V_g. The device is a 13 nm thick, 7 µm wide, and 5 µm long b-PC p-FET measured at $V_d = 100$ mV with different cryogenic temperatures ranging from 30 to 280 K. The doping cycle of this device is 20. $G = I_d / V_d$. d) The hole carrier density of the same b-PC p-FET described in panel (c) as a function of temperature (T) measured at various back gate voltage V_g. $V_d = 100$ mV (see the Supporting Information for computation of carrier density). e) The dependence of the FE p-type mobility on the operating temperature (T). Device was measured at $V_d = 100$ mV. Same device as in panel (c).

TOF-SIMS confirms the presence of the allotropes of phosphorus carbide predicted by theoretical calculations. Additionally, a low contact resistance of 289 Ω µm was achieved via a NiP alloy contact with an edge contacted metal/PC interface at the source/drain made possible by sputtering and thermal treatment.

Supporting Information

Supporting Information is available from the Wiley Online Library or from the author.

Acknowledgements

This research was supported by the National University of Singapore Faculty Research Committee Grants (R-263-000-B21-133 and R-263-000-B21-731), A*STAR Science and Engineering ResearchCouncil Grants (152-70-00013 and 152-70-00017), and by the National Research Foundation, Prime Minister's Office, Singapore under its medium sized centre program. The authors thank Kuan Henche in the Department of Materials Science and Engineering at NUS for assisting with the XPS measurements. The authors thank Prof. Chengkuo Lee and Dihan Md Nuruddin Hasan in the Department of Electrical Engineering at NUS, and Nor Ibrahim Bin Mohd Nor and Marcos Vinicius Surmani Martins at the Centre for Advanced 2D Materials of NUS for assisting with the FTIR measurements.

Conflict of Interest

The authors declare no conflict of interest.

Keywords

alloyed contacts, black phosphorus carbide, carbon doping, field-effect transistors, mobility

Received: January 24, 2017
Revised: March 1, 2017
Published online:

[1] F. Schwierz, *Nat. Nano* **2010**, *5*, 487.
[2] S. Some, J. Kim, K. Lee, A. Kulkarni, Y. Yoon, S. Lee, T. Kim, H. Lee, *Adv. Mater.* **2012**, *24*, 5481.
[3] D. Jariwala, V. K. Sangwan, L. J. Lauhon, T. J. Marks, M. C. Hersam, *ACS Nano* **2014**, *8*, 1102.
[4] Q. Weng, X. Wang, X. Wang, Y. Bando, D. Golberg, *Chem. Soc. Rev.* **2016**, *45*, 3989.
[5] B. Liu, M. Köpf, A. N. Abbas, X. Wang, Q. Guo, Y. Jia, F. Xia, R. Weihrich, F. Bachhuber, F. Pielnhofer, H. Wang, R. Dhall, S. B. Cronin, M. Ge, X. Fang, T. Nilges, C. Zhou, *Adv. Mater.* **2015**, *27*, 4423.
[6] X. Ling, H. Wang, S. Huang, F. Xia, M. S. Dresselhaus, *Proc. Natl. Acad. Sci. USA* **2015**, *112*, 4523.
[7] Z.-C. Luo, M. Liu, Z.-N. Guo, X.-F. Jiang, A.-P. Luo, C.-J. Zhao, X.-F. Yu, W.-C. Xu, H. Zhang, *Opt. Express* **2015**, *23*, 20030.
[8] S. B. Lu, L. L. Miao, Z. N. Guo, X. Qi, C. J. Zhao, H. Zhang, S. C. Wen, D. Y. Tang, D. Y. Fan, *Opt. Express* **2015**, *23*, 11183.
[9] Z.-P. Ling, J.-T. Zhu, X. Liu, K.-W. Ang, *Sci. Rep.* **2016**, *6*, 26609.
[10] L. Li, M. Engel, D. B. Farmer, S.-J. Han, H. S. P. Wong, *ACS Nano* **2016**, *10*, 4672.
[11] Z.-P. Ling, S. Sakar, S. Mathew, J.-T. Zhu, K. Gopinadhan, T. Venkatesan, K.-W. Ang, *Sci. Rep.* **2015**, *5*, 18000.
[12] G. Long, D. Maryenko, J. Shen, S. Xu, J. Hou, Z. Wu, W. K. Wong, T. Han, J. Lin, Y. Cai, R. Lortz, N. Wang, *Nano Lett.* **2016**, *16*, 7768.
[13] H. Liu, A. T. Neal, M. Si, Y. Du, P. D. Ye, *IEEE Electron Device Lett.* **2014**, *35*, 795.
[14] a) F. Xia, H. Wang, Y. Jia, *Nat. Commun.* **2014**, *5*, 4458; b) H. Liu, A. T. Neal, Z. Zhu, Z. Luo, X. Xu, D. Tománek, P. D. Ye, *ACS Nano* **2014**, *8*, 4033.
[15] S. P. Koenig, R. A. Doganov, L. Seixas, A. Carvalho, J. Y. Tan, K. Watanabe, T. Taniguchi, N. Yakovlev, A. H. Castro Neto, B. Özyilmaz, *Nano Lett.* **2016**, *16*, 2145.
[16] S. Das, M. Demarteau, A. Roelofs, *ACS Nano* **2014**, *8*, 11730.
[17] Y. Du, H. Liu, Y. Deng, P. D. Ye, *ACS Nano* **2014**, *8*, 10035.
[18] L. Li, Y. Yu, G. J. Ye, Q. Ge, X. Ou, H. Wu, D. Feng, X. H. Chen, Y. Zhang, *Nat. Nanotechnol.* **2014**, *9*, 372.
[19] D. J. Perello, S. H. Chae, S. Song, Y. H. Lee, *Nat. Commun.* **2015**, *6*, 7809.
[20] G. Wang, R. Pandey, S. P. Karna, *Nanoscale* **2016**, *8*, 8819.
[21] J. Guan, D. Liu, Z. Zhu, D. Tománek, *Nano Lett.* **2016**, *16*, 3247.
[22] S. R. J. Pearce, P. W. May, R. K. Wild, K. R. Hallam, P. J. Heard, *Diamond Relat. Mater.* **2002**, *11*, 1041.
[23] F. Claeyssens, G. M. Fuge, N. L. Allan, P. W. May, M. N. R. Ashfold, *Dalton Trans.* **2004**, *19*, 3085.
[24] G. Kresse, J. Furthmüller, *Phys. Rev. B* **1996**, *54*, 11169.
[25] T. R. Gow, R. Lin, L. A. Cadwell, F. Lee, A. L. Backman, R. I. Masel, *Chem. Mater.* **1989**, *1*, 406.
[26] J. Sun, G. Zheng, H.-W. Lee, N. Liu, H. Wang, H. Yao, W. Yang, Y. Cui, *Nano Lett.* **2014**, *14*, 4573.
[27] Y. Wen, B. Wang, C. Huang, L. Wang, D. Hulicova-Jurcakova, *Chem. - Eur. J.* **2015**, *21*, 80.
[28] C. R. Ryder, J. D. Wood, S. A. Wells, Y. Yang, D. Jariwala, T. J. Marks, G. C. Schatz, M. C. Hersam, *Nat. Chem.* **2016**, *8*, 597.
[29] N. B. Goodman, L. Ley, D. W. Bullett, *Phys. Rev. B* **1983**, *27*, 7440.
[30] J. D. Wood, S. A. Wells, D. Jariwala, K.-S. Chen, E. Cho, V. K. Sangwan, X. Liu, L. J. Lauhon, T. J. Marks, M. C. Hersam, *Nano Lett.* **2014**, *14*, 6964.
[31] A. N. Rudenko, S. Brener, M. I. Katsnelson, *Phys. Rev. Lett.* **2016**, *116*, 246401.